A Solvable Contact Potential Based on a Nuclear Model

A. Martín-Mozo, L.M. Nieto and C. Romaniega

Departamento de Física Teórica, Atómica y Óptica and IMUVA, Universidad de Valladolid, 47011. Valladolid, Spain

Abstract. We extend previous works on the study of a particle subject to a three-dimensional spherical singular potential including a δ-δ' contact interaction. In this case, to have a more realistic model, we add a Coulombic term to a finite well and a radial δ-δ' contact interaction just at the edge of the well, which is where the surface of the nucleus would be. We first prove that the we are able to define the contact potential by matching conditions for the radial function, fixing a self-adjoint extension of the non-singular Hamiltonian. With these matching conditions, we are able to find analytic solutions of the wave function and focus the analysis on the bound state structure characterizing and computing the number of bound states. For this approximation for a mean-field Woods-Saxon model, the Coulombic term enables us to complete the previous study for neutrons analyzing the proton energy levels in some doubly magic nuclei. In particular, we find the appropriate δ' contribution fitting the available data for the neutron and proton level schemes of the nuclei ^{208}Pb, ^{40}Ca, and ^{16}O.

PACS. 02.30.Em Potential theory – 03.65.–w Quantum mechanics

1 Introduction

The present work generalizes the model introduced in a recent publication in which the energy levels of neutrons in doubly magical nuclei were studied [1]. The analysis carried out there is taken a step further by introducing a Coulombic term so that we can study the neutron and proton level scheme. Both models are based on the introduction of singular potentials supported on a sphere of radius R, indeed a δ-δ' contact interaction which generalizes the Dirac δ. Within the Woods-Saxon model, the aforementioned interaction arises if we make the parameter that describes the surface diffuseness of the nucleus go to zero, which naturally leads to the description of the spin-orbit coupling by the Dirac δ potential. To improve the approximation on surface diffuseness, the δ' interaction will be adapted to fit the available data for nucleon energy levels. Within this framework, we can avoid numerical methods for calculating wave functions and we can study the properties of the energy level scheme using the characteristics of the special functions that are the solutions of the corresponding Schrödinger equation. Another approach to obtain analytic solutions is based on the Nikiforov–Uvarov method, applied in [2] to obtain the neutron level scheme. In this case the approximation consists in the expansion of the centrifugal and Woods-Saxon terms of the potential in a series of exponentials and keeping the terms up to second order.

The main advantage of these contact potentials is that they can often be resolved exactly, which gives a good insight of some quantum properties. This is why these interactions have a large number of applications in the modeling of real physical systems, some of which are listed in [1] and the references quoted therein [3–13]. In this regard, it is worth mentioning a recent work in which the vacuum interaction energy of a three-dimensional scalar field is calculated in the presence of two concentric spheres defined by the aforementioned contact interaction [14], so that the δ' term leads to positive Casimir interaction energies, which are unattainable only with the Dirac δ.

In our work, the δ' term will be used as part of the phenomenological potential, its definition being fully justified in the text, based on the fact that spherically symmetric three-dimensional Schrödinger equations admit a one-dimensional counterpart for each value of the orbital angular momentum. When working with this radial equation, the δ-δ' interaction supported on the sphere becomes a one-dimensional interaction supported on a point. Regarding the δ-δ' interaction, it is constructed by establishing a self-adjoint determination of the Hamiltonian without the singular term [15]. The determination of the self-adjoint extension, that is, the definition of the δ-δ' interaction, is given by the use of suitable matching conditions for the wave functions at the radius. In this sense, although the δ interaction is universally accepted, the same is not the case for the δ' term, for which there are at least two definitions that are consistent with its desirable properties [16,17]. These matching conditions determine a domain in which the Hamiltonian with the δ' interaction is self-adjoint [18]. In this paper, following the lines developed in [15,19], we will

use the so called *local δ'* interaction since it is compatible with the δ potential when both interactions are supported on the same point. This condition arises naturally from the proposed model and furthermore, this interaction can be seen as a generalization of the Robin boundary conditions, which can be obtained as a finite limit case [20].

Although the formalism developed here is valid for any non-relativistic particle subject to a three-dimensional spherical potential consisting of a Coulombic term, a finite well, and a radial δ-δ' contact interaction at the edge of the well, our main motivation is to analyze the already mentioned nuclear mean field potential. In fact, the Dirac δ interaction has been used for the calculation of resonant parameters and energy spectrum in [21], and it has also been employed to study the spectral function of the unbound nucleus ^{25}O [22]. Following the work [1], we now study the energy levels of protons and compare them with those of neutrons in the previous paper. As we will see, the general properties of the structure of the level scheme are maintained, although there are certain differences due to the Coulombic term.

The article is organized as follows. In Section 2, we introduce the potential under consideration, which is written to be well suited for future application to a nuclear model. The radial δ and δ' terms appear here explicitly. In Section 3, we derive the secular equation for which the solutions give the bound states. In Section 4, we study the existence and localization of bound states, the energy levels, and we will see that the general properties of spherical potentials hold with respect to quantum numbers. These findings are tested with available data of the nucleus ^{208}Pb in Section 5, where we explicitly compare the proton level scheme with the neutron level scheme. We also calculate the coupling of the δ' interaction that best fits the data available for this nucleus. The same procedure can be applied to other doubly magic nuclei and therefore in Appendix A we provide useful data for all known doubly magic nuclei and in Appendix B the level scheme and the optimized value of the δ' coupling for the isotopes ^{16}O and ^{40}Ca. The article ends with some final remarks.

2 Model and motivation

In this section we introduce the model under study. Although we have used a suitable notation for possible applications in nuclear physics, as in [1], any non-relativistic quantum particle can be analyzed within this framework. The starting point is the following single-particle three-dimensional Hamiltonian, written with respect to the coordinates of the center of mass of the system,

$$H(\mathbf{r}) = -\frac{\hbar^2}{2\mu}\nabla_{\mathbf{r}}^2 + U_0(r) + U_{\mathrm{so}}(r)(\mathbf{L}\cdot\mathbf{S}) + U_{\mathrm{q}}(r) + V_{\mathrm{C}}(r), \tag{1}$$

where μ is the reduced mass and $U_0(r)$, $U_{\mathrm{so}}(r)$, and $U_{\mathrm{q}}(r)$ are, essentially, the Woods-Saxon potential [23], its first and second derivative, respectively:

$$U_0(r) = -V_0\,f(r) = -V_0\,\frac{1}{1+e^{(r-R)/a}}, \tag{2}$$

$$U_{\mathrm{so}}(r) = \frac{V_{\mathrm{so}}}{\hbar^2}\,f'(r) = -\frac{V_{\mathrm{so}}}{a\hbar^2}\,\frac{e^{(r-R)/a}}{\left(1+e^{(r-R)/a}\right)^2}, \tag{3}$$

$$U_{\mathrm{q}}(r) = V_{\mathrm{q}}\,f''(r) = -\frac{V_{\mathrm{q}}}{a^2}\,\frac{e^{(r-R)/a}\left(1-e^{(r-R)/a}\right)}{\left(1+e^{(r-R)/a}\right)^3}. \tag{4}$$

The Coulombic potential is the static Coulomb potential of a uniformly charged sphere of radius R and therefore depends on the radial variable differently inside and outside the nucleus:

$$V_{\mathrm{C}}(r) = \frac{Ze^2}{4\pi\epsilon_0}\begin{cases}\dfrac{3-(r/R)^2}{2R}, & r \leq R, \\[2mm] \dfrac{1}{r}, & r > R,\end{cases} \tag{5}$$

where Z is the number of protons. As already mentioned, in Ref. [1] only neutron energy levels were studied, so this Coulombic potential (5) was not included in the Hamiltonian. We now study the connection between the strength which appears in the radial interaction (2)-(4) and real physical parameters [24–26]. Note that the strengths of the Woods-Saxon potential (V_0) and the spin-orbit term (V_{so}) must be positive defined to reproduce the experimental magic numbers [27]. However, the sign and value of V_{q} can be selected to fit the available data, as we will see later in Sec. 5. Here we will use the usual parametrization of the nuclear radius R, which for this phenomenological potential is given as a function of the nuclear mas $A = N + Z$ as $R = r_0 A^{1/3}$, being r_0 a constant and N the number of neutrons. The parameter a gives the thickness of the surface of $f(r)$. A typical value for this parameter is $a = 0.7$ fm [28].

Following the same steps as in [1], we first substitute the Laplacian in the Hamiltonian (1) in terms of the orbital angular momentum $\mathbf{L}$ and the radial coordinates,

$$-\frac{\hbar^2}{2\mu}\nabla_{\mathbf{r}}^2 = -\frac{\hbar^2}{2\mu}\left[\frac{1}{r^2}\frac{\partial}{\partial r}\left(r^2\frac{\partial}{\partial r}\right) - \frac{\mathbf{L}^2/\hbar^2}{r^2}\right]. \tag{6}$$

Then, as usual, the eigenfunctions of the corresponding stationary three-dimensional Schrödinger equation are factored into a radial part $u_{n\ell j}(r)/r$ and an angular part $\mathcal{Y}_{\ell jm}(\theta, \phi)$. The latter fulfills

$$\mathbf{L}^2\mathcal{Y}_{\ell jm}(\theta, \phi) = \hbar^2\,\ell(\ell+1)\mathcal{Y}_{\ell jm}(\theta, \phi), \qquad (\mathbf{L}\cdot\mathbf{S})\,\mathcal{Y}_{\ell jm}(\theta, \phi) = \hbar^2\,\xi_{\ell j}\,\mathcal{Y}_{\ell jm}(\theta, \phi). \tag{7}$$

The function $\mathcal{Y}_{\ell jm}(\theta, \phi)$, a linear combination of spherical harmonics $Y_{\ell m}(\theta, \phi)$, is a simultaneous eigenfunction of the operators $\mathbf{L}^2$, $\mathbf{S}^2$, $\mathbf{J}^2 = (\mathbf{L}+\mathbf{S})^2$ and J_z [28]. We have also introduced the constants $\xi_{\ell j} = \frac{1}{2}(j(j+1) - \ell(\ell+1) - \frac{3}{4})$:

$$\xi_{\ell j} = \begin{cases} \ell/2 & \text{for } j = \ell + \frac{1}{2}, \\ -(\ell+1)/2 & \text{for } j = \ell - \frac{1}{2}, \end{cases} \tag{8}$$

where ℓ takes values in the non-negative integers $\mathbb{N}_0$. For $\ell = 0$ the only possibility is $j = 1/2$ so $\xi_{0j} = 0$. Using the previous relationships, the radial part fulfills $Hu_{n\ell j}(r) = E_{n\ell j}\,u_{n\ell j}(r)$, where

$$H = \frac{-\hbar^2}{2\mu}\left[\frac{\mathrm{d}^2}{\mathrm{d}r^2} - \frac{\ell(\ell+1)}{r^2}\right] - V_0 f(r) + V_{\mathrm{so}}\xi_{\ell j}f'(r) + V_{\mathrm{q}}f''(r) + V_{\mathrm{C}}(r). \tag{9}$$

Finally, to arrive at the explicit form of the effective potential that will be used later, we take here the limit $a \to 0^+$. First, note that

$$\lim_{a\to 0^+} U_0(r) = \begin{cases} -V_0 & \text{if } r < R \\ -V_0/2 & \text{if } r = R \\ 0 & \text{if } r > R \end{cases} = V_0\left[\theta(r-R) - 1\right], \tag{10}$$

where $\theta(x)$ is the Heaviside step function. The function $f(r)$ can be seen as a distribution in a certain space of test functions, such as the Schwartz space. Then, if $\psi(r)$ is an arbitrary function of this space, we denote the action of the distribution $f(r)$ on $\psi(r)$ by $\langle \psi(r)|f(r)\rangle = \int_0^\infty \psi^*(r)\,f(r)\,dr$. For the first derivative of $f(r)$ we obtain the limit

$$\lim_{a\to 0^+}\left\langle \psi(r)\left|\frac{\mathrm{d}}{\mathrm{d}r}f(r)\right.\right\rangle = -\lim_{a\to 0^+}\langle\psi'(r)|f(r)\rangle = -\langle\psi'(r)|1 - \theta(r-R)\rangle = \langle\psi(r)| - \delta(r-R)\rangle. \tag{11}$$

This is valid since, from the point of view of distributions, the Dirac δ is the derivative of the Heaviside step function. Hence,

$$\lim_{a\to 0^+} V_{\mathrm{so}}\,\xi_{\ell j}\,f'(r) = -V_{\mathrm{so}}\,\xi_{\ell j}\,\delta(r-R). \tag{12}$$

In the same way, we obtain the following expression for the second derivative of $f(r)$:

$$\lim_{a\to 0^+} U_{\mathrm{q}}(r) = \lim_{a\to 0^+} V_{\mathrm{q}}f''(r) = -V_{\mathrm{q}}\,\delta'(r-R). \tag{13}$$

In view of these considerations, the Hamiltonian (9) in the limit $a \to 0^+$ becomes

$$H_{\mathrm{sing}} = -\frac{\hbar^2}{2\mu}\left[\frac{\mathrm{d}^2}{\mathrm{d}r^2} - \frac{\ell(\ell+1)}{r^2}\right] + V_0[\theta(r-R) - 1] - V_{\mathrm{so}}\xi_{\ell j}\delta(r-R) - V_{\mathrm{q}}\delta'(r-R) + V_{\mathrm{C}}(r), \tag{14}$$

where the singular (contact) terms are already included. Taking into account that $R \gg a$, we can consider the simplified one-dimensional Hamiltonian (14) above as a mean-field potential to describe the energy levels of protons and neutrons. The main advantage of using (14) is that the eigenvalue equation $H_{\mathrm{sing}}u_{n\ell j}(r) = E_{n\ell j}u_{n\ell j}(r)$ can be solved exactly for the wave function in terms of hypergeometric functions Hereinafter, for simplicity and when no confusion arises, we will use as shorthand notation $u_\ell \equiv u_{n\ell j}$.

As explained in the first appendix of [1], the δ-δ' perturbation in (14) is defined using the formalism of self-adjoint extensions of symmetric (formally Hermitian) operators with equal deficiency indices. This gives two options for the meaning of δ' term. One is a δ' which is often called the *non-local* δ' [16], but this choice is incompatible with the Dirac δ [17]. The other possibility, the one we will adopt, is called *local* δ' and is defined by matching conditions established at the point supporting the interaction.

3 Solutions of the singular Schrödinger equation

In this section we determine the eigenfunctions corresponding to the bound states of the singular Hamiltonian (14),

$$\left[-\frac{d^2}{dr^2} + \frac{\ell(\ell+1)}{r^2} - \frac{2\mu E}{\hbar^2} + \frac{2\mu V_0}{\hbar^2}(\theta(r-R)-1) + \frac{2\mu}{\hbar^2}V_C(r) + \alpha_{\ell j}\delta(r-R) + \beta\delta'(r-R) \right] u_\ell(r) = 0, \qquad (15)$$

where we have defined the new parameters

$$\alpha_{\ell j} = -2\mu\, V_{so}\, \xi_{\ell j}/\hbar^2, \qquad \beta = -2\mu\, V_q/\hbar^2\,. \qquad (16)$$

It should be noted that we can consider the parameters $\alpha_{\ell j}$ and β as two independent coefficients, unrelated to any future application to a nuclear model. Therefore, the equation (15) can be analyzed for a generic quantum particle subjected to a spherical well, with a δ-δ' interaction at the edge and a Coulombic term. The radial Schrödinger equation (15) is defined on the interval $0 \le r < \infty$. To solve it, due to the presence of the contact potential, we divide this semi-axis into two regions: $0 \le r < R$ and $R < r$. We will obtain the wave function in each region and then apply the appropriate matching conditions on $r = R$, thus defining the singular part of the Hamiltonian.

3.1 Interior wave equation

For the study of solutions in the region $0 \le r < R$, we consider energy values $E > -V_0$. Hence, we must solve the differential equation

$$\left[-\frac{d^2}{dr^2} + \frac{\ell(\ell+1)}{r^2} - \frac{2\mu(E+V_0)}{\hbar^2} + \frac{2\mu}{\hbar^2}\frac{Ze^2}{4\pi\epsilon_0}\frac{3-(r/R)^2}{2R} \right] u_\ell(r) = 0. \qquad (17)$$

First, we make the following changes to the parameters that appear in (17),

$$g \equiv \sqrt{\frac{\mu Ze^2 R}{4\pi\hbar^2\epsilon_0}}, \quad \kappa \equiv \frac{R^2}{4g}\left[\frac{2\mu(E+V_0)}{\hbar^2} - \frac{3g^2}{R^2} \right], \quad z \equiv (-ig/R^2)r^2, \qquad (18)$$

and then, based on the asymptotic behavior of the solutions of (17), we propose the following change in the unknown wave function:

$$u_\ell(r) = r^{\ell+1}\exp\left(\frac{igr^2}{2R^2} \right)\omega_\ell(z), \qquad (19)$$

With this, Eq. (17) is transformed into a Kummer differential equation:

$$z\frac{d^2\omega_\ell(z)}{dz^2} + \left(\ell + \frac{3}{2} - z \right)\frac{d\omega_\ell(z)}{dz} - \left[\frac{1}{2}\left(\ell + \frac{3}{2} \right) - i\kappa \right]\omega_\ell(z) = 0. \qquad (20)$$

For each particular value of the orbital angular momentum ℓ, the general solution of (20) is given by

$$\omega_\ell(z) = A_\ell\, {}_1F_1\left(a, c; z \right) + B_\ell\, z^{1-c}\, {}_1F_1\left(a+1-c, 2-c; z \right), \qquad (21)$$

where ${}_1F_1$ denotes the Kummer function, A_ℓ, B_ℓ are arbitrary constants, and

$$a \equiv \frac{1}{2}\left(\ell + \frac{3}{2} \right) - i\kappa, \qquad c \equiv \ell + \frac{3}{2}. \qquad (22)$$

Note that the two solutions are linearly independent since $c \notin \mathbb{Z}$ for any ℓ. In fact, the second solution is not square integrable near zero due to the factor z^{1-c}. On the other hand, from the definition of ${}_1F_1$ it is obvious that this function is equal to one at the origin and therefore it is square integrable on the finite interval considered. Consequently, the admissible solutions are precisely

$$u_\ell(r) = A_\ell\, r^{\ell+1}e^{igr^2/2R^2}\, {}_1F_1\left(\frac{1}{2}\left(\ell + \frac{3}{2} \right) - i\kappa, \ell + \frac{3}{2}; \frac{-igr^2}{R^2} \right), \quad 0 \le r < R. \qquad (23)$$

3.1.1 Neutron case

Let us investigate now the limit $Z \to 0$ as a consistency test of Eq. (23), that can be rewritten as [29]

$$u_\ell(r) = A_\ell r^{\ell+1} e^{igr^2/2R^2} \sum_{k=0}^{\infty} \frac{\left(\frac{1}{2}\left(\ell+\frac{3}{2}\right)-i\kappa\right)_k}{\left(\ell+\frac{3}{2}\right)_k k!} \left(-\frac{ig}{R^2}\right)^k r^{2k}, \tag{24}$$

where $(x)_n$ denotes the Pochhammer symbol. Consequently, we can evaluate

$$\lim_{Z \to 0} u_\ell(r) = A_\ell \sum_{k=0}^{\infty} r^{\ell+1} \frac{\left(-\frac{\sigma^2}{2^2}\right)^k}{\left(\ell+\frac{3}{2}\right)_k k!} r^{2k} = \left[\frac{2^{\ell+1} A_\ell \Gamma\left(\ell+\frac{3}{2}\right)}{\sigma^{\ell+1}}\right] \sum_{k=0}^{\infty} \frac{(-1)^k}{\Gamma\left(\ell+\frac{3}{2}+k\right) k!} \left(\frac{\sigma r}{2}\right)^{2k+\ell+1}. \tag{25}$$

On the other hand, the solution obtained in [1] for $r < R$ was

$$y_\ell(r) = A'_\ell \sqrt{\sigma r}\, J_{\ell+\frac{1}{2}}(\sigma r), \qquad \sigma = \sqrt{\mu(E+V_0)}/\hbar, \tag{26}$$

where J_ν denotes the Bessel function of the first kind. From its definition as a power of series, (26) is equivalent to

$$y_\ell(r) = \sqrt{2}\, A'_\ell \sum_{k=0}^{\infty} \frac{(-1)^k}{\Gamma(k+\ell+\frac{3}{2})k!} \left(\frac{\sigma r}{2}\right)^{2k+\ell+1}. \tag{27}$$

Therefore, the limit of $u_\ell(r)$ in (34) is essentially the result obtained in [1], as expected.

3.2 Exterior wave equation

For values of r such that $R < r$, we have to solve the Schrödinger equation (15) for $V_0 = 0$. Since we are looking for bound states, we require $E < 0$. We should solve

$$\frac{d^2 u_\ell(r)}{dr^2} + \left[\frac{2\mu E}{\hbar^2} - \frac{2g^2}{rR} - \frac{\ell(\ell+1)}{r^2}\right] u_\ell(r) = 0. \tag{28}$$

First of all we proceed to make the change of variables $x = \eta r$, $u_\ell(r) \equiv v_\ell(x)$, being

$$\eta \equiv \sqrt{\frac{8\mu|E|}{\hbar^2}}, \qquad \lambda \equiv -\frac{2g^2}{\eta R} = -\frac{\sqrt{\mu}Ze^2}{2\pi\hbar\varepsilon_0\sqrt{8|E|}}. \tag{29}$$

With this, equation (28) becomes a Whittaker differential equation

$$\frac{d^2 v_\ell(x)}{dx^2} + \left[\frac{\lambda}{x} - \frac{1}{4} - \frac{\ell(\ell+1)}{x^2}\right] v_\ell(x) = 0. \tag{30}$$

For each particular value of the orbital angular momentum ℓ, its general solution is given by

$$u_\ell(r) = C_\ell M_{\lambda,\ell+\frac{1}{2}}(\eta r) + D_\ell W_{\lambda,\ell+\frac{1}{2}}(\eta r), \tag{31}$$

where $M_{\chi,\gamma}$ and $W_{\chi,\gamma}$ denote the Whittaker functions [29], with C_ℓ and D_ℓ being arbitrary constants. Again, if we are looking for square integrable solutions, we need to know the asymptotic behaviors of these functions for large values of r, which are,

$$M_{\lambda,\ell+\frac{1}{2}}(\eta r) \sim \Gamma(2+2\ell)e^{\frac{1}{2}\eta r}(\eta r)^{-\lambda}/\Gamma(1+\ell-\lambda), \qquad W_{\lambda,\ell+\frac{1}{2}}(\eta r) \sim e^{-\frac{1}{2}\eta r}(\eta r)^\lambda. \tag{32}$$

Consequently, the solution (31) is square integrable if, and only if, $C_\ell = 0$. In this way, the only possible contribution comes from the second term, so that

$$u_\ell(r) = D_\ell W_{\lambda,\ell+\frac{1}{2}}(\eta r), \quad r > R. \tag{33}$$

3.2.1 Neutron case

Again, we investigate the limit $Z, \lambda \to 0$ as a consistency test of Eq. (33), giving

$$\lim_{Z \to 0} u_\ell(r) = D_\ell \, W_{0,\ell+\frac{1}{2}}(\eta r). \tag{34}$$

On the other hand, the solution obtained in [1] for $r > R$ was

$$u_\ell(r) = D_\ell \sqrt{\frac{\eta r}{2}} \, K_{\ell+\frac{1}{2}} \left(\frac{\eta r}{2} \right), \tag{35}$$

where K_ν denotes the modified Bessel function of the second kind, which fulfills [29]

$$\sqrt{\frac{2z}{\pi}} K_\nu(z) = W_{0,\nu}(2z), \tag{36}$$

so it coincides with the limit just obtained in (34), as expected.

3.3 Matching conditions

Once we have obtained the inner and outer solutions, we need to link both at $r = R$ in a proper way. As established by the standard literature on the subject [18], there are requirements for the reduced radial function at the point $r = R$ that fix a self-adjoint determination of the operator

$$H_r \equiv -\frac{\mathrm{d}^2}{\mathrm{d}r^2} + \frac{\ell(\ell+1)}{r^2} + \frac{2\mu V_0}{\hbar^2}[\theta(r-R) - 1] + \frac{2\mu}{\hbar^2} V_C(r), \tag{37}$$

thus defining the final Hamiltonian of Eq. (15). These requirements are given by matching conditions that relate the values of the function $u_\ell(r)$ and its first derivative at R, and can be written in terms of a $SL(2, \mathbb{R})$ matrix as [20,30,31]

$$\begin{pmatrix} u_\ell(R^+) \\ u'_\ell(R^+) \end{pmatrix} = \begin{pmatrix} \dfrac{2+\beta}{2-\beta} & 0 \\ \dfrac{4\alpha_{\ell j}}{4-\beta^2} & \dfrac{2-\beta}{2+\beta} \end{pmatrix} \begin{pmatrix} u_\ell(R^-) \\ u'_\ell(R^-) \end{pmatrix}, \quad \text{where} \quad u_\ell(R^\pm) = \lim_{x \to R^\pm} u_\ell(x). \tag{38}$$

The function $u_\ell(r)$ is given by (23) and (33). There is a rigorous discussion on the self-adjointness of H_r with $Z = 0$ in Appendix A of [1]. In the latter, the appropriate domain in which the one-dimensional operator (37) with $Z = 0$ admits a four parameter family of self-adjoint extensions for a fixed value of ℓ is found. With this in mind, this Hamiltonian plus the δ-δ' interaction was defined using the formalism of self-adjoint extensions of symmetric operators with equal deficiency indices. The same procedure is valid for $Z > 0$. To show that adding $V_C(r)$ to the aforementioned Hamiltonian in [1] does not change the self-adjointness, we use the Kato-Rellich theorem. More precisely, since $V_C(r)$ is bounded and Hermitian, we can state that the complete Hamiltonian is self-adjoint [32].

It should be noted that for $\beta = \pm 2$, the above matching conditions are no longer applicable and in this case the respective self-adjoint extensions of the radial Hamiltonian are given by the following boundary conditions at $r = R$ [30]

$$u_\ell(R^+) - \frac{4}{\alpha_{\ell j}} u'_\ell(R^+) = 0, \qquad u_\ell(R^-) = 0, \quad \text{if} \quad \beta = 2,$$
$$\tag{39}$$
$$u_\ell(R^-) + \frac{4}{\alpha_{\ell j}} u'_\ell(R^-) = 0, \qquad u_\ell(R^+) = 0, \quad \text{if} \quad \beta = -2.$$

Using (23) and (33), the matrix relation (38) yields the following secular equation:

$$\frac{4iag}{3+2\ell} \frac{{}_1F_1(a+1, b+1; -ig)}{{}_1F_1(a, b; -ig)} = 1 + \ell + ig + \frac{w_{\ell j}}{(2-\beta)^2} - \frac{(2+\beta)^2}{(2-\beta)^2}\left[\frac{\eta R}{2} - \lambda - \frac{W_{\lambda+1,\ell+\frac{1}{2}}(\eta R)}{W_{\lambda,\ell+\frac{1}{2}}(\eta R)} \right], \tag{40}$$

where we have introduced the dimensionless quantities v_0, $w_{\ell j}$, ε and the constant g, already defined in Eq. (18):

$$v_0 \equiv \sqrt{\frac{2\mu R^2 V_0}{\hbar^2}}, \qquad w_{\ell j} \equiv 4\alpha_{\ell j} R, \qquad \varepsilon \equiv \frac{|E|}{V_0} \in (0,1), \qquad g \equiv \sqrt{\frac{\mu Z e^2 R}{4\pi \hbar^2 \epsilon_0}}. \tag{41}$$

Then previously handled variables can be rewritten based on these as

$$\kappa = \frac{v_0^2}{4g}(1 - \varepsilon) - \frac{3}{4}g, \quad a = \frac{1}{2}\left(\ell + \frac{3}{2}\right) - \frac{i}{4}\left(\frac{v_0^2}{4g}(1 - \varepsilon) - 3g\right), \quad \eta = \frac{2v_0}{R}\sqrt{\varepsilon}, \quad \lambda = -\frac{g^2}{v_0\sqrt{\varepsilon}}. \tag{42}$$

We will denote the left side of (40) by $\varphi_\ell(\varepsilon)$ and the right side by $\phi_\ell(\varepsilon)$ (which also depends on j and β), that is,

$$\varphi_\ell(\varepsilon) \equiv \frac{4iag}{3 + 2\ell} \frac{{}_1F_1(a + 1, \ell + \frac{5}{2}; -ig)}{{}_1F_1(a, \ell + \frac{3}{2}; -ig)}, \tag{43}$$

$$\phi_\ell(\varepsilon) \equiv 1 + \ell + ig + \frac{w_{\ell j}}{(2 - \beta)^2} - \frac{(2 + \beta)^2}{(2 - \beta)^2}\left[\frac{\eta R}{2} - \lambda - \frac{W_{\lambda+1,\ell+\frac{1}{2}}(\eta R)}{W_{\lambda,\ell+\frac{1}{2}}(\eta R)}\right]. \tag{44}$$

Note that $\operatorname{Im}[\phi_\ell] = g$ since the Whittaker functions are real, and therefore $\operatorname{Im}[\varphi_\ell] = g$ for the left side of (40). In the situation we are analyzing, the first difference with the neutron case [1] is precisely the imaginary part that appears in the secular equation (40), although, as we will see, this fact does not alter the solutions obtained from the real part. In order to prove it, we first derive the following result on Kummer's functions.

Proposition 1 *For any $x, y, z \in \mathbb{R}$, the following relation holds*

$$\operatorname{Re}\left[\frac{(x + iy)\,{}_1F_1(x + iy + 1, 2x + 1; -iz)}{x\,{}_1F_1(x + iy, 2x; -iz)}\right] = 1, \tag{45}$$

being ${}_1F_1$ the Kummer function.

Proof Using Kummer's first transformation formula [29], we have

$${}_1F_1(a, b; z) = e^z{}_1F_1(b - a, b; -z). \tag{46}$$

If we define $M(x, y, z) \equiv {}_1F_1(x + iy, 2x; -iz)$, from the previous equation we obtain

$$M(x, y, z) \equiv {}_1F_1(x + iy, 2x; -iz) = e^{-iz}{}_1F_1(x - iy, 2x; iz) \equiv e^{-iz}M^*(x, y, z), \tag{47}$$

where w^* denotes complex conjugation. Consequently, $\ln M - \ln M^* = -iz$ and

$$\left[\frac{\mathrm{d}}{\mathrm{d}z}\ln M\right] - \left[\frac{\mathrm{d}}{\mathrm{d}z}\ln M\right]^* = 2i\operatorname{Im}\left[\frac{\mathrm{d}}{\mathrm{d}z}\ln M\right] = -i. \tag{48}$$

Therefore

$$\operatorname{Re}\left[2i\frac{\mathrm{d}}{\mathrm{d}z}\ln{}_1F_1(x + iy, 2x; -iz)\right] = 1. \tag{49}$$

The proof is concluded noting that the logarithmic derivative of this function satisfies [29]

$$2i\frac{\mathrm{d}}{\mathrm{d}z}\ln{}_1F_1(x + iy, 2x; -iz) = \frac{(x + iy)\,{}_1F_1(x + iy + 1, 2x + 1; -iz)}{x\,{}_1F_1(x + iy, 2x; -iz)}. \quad \blacksquare \tag{50}$$

In our case, taking

$$z = g, \qquad x = \frac{1}{2}\left(\ell + \frac{3}{2}\right) = \frac{b}{2}, \qquad y = -\kappa, \quad \Rightarrow \quad a = x + iy, \tag{51}$$

the left side of the secular equation can be written as

$$\varphi_\ell(\varepsilon) = \frac{4iag}{3 + 2\ell} \frac{{}_1F_1(a + 1, b + 1; -ig)}{{}_1F_1(a, b; -ig)} = g\frac{i\,(x + iy)\,{}_1F_1(x + iy + 1, 2x + 1; -iz)}{x\,{}_1F_1(x + iy, 2x; -iz)}.$$

Finally, from Proposition 1:

$$\operatorname{Im}[\varphi_\ell] = -\operatorname{Re}[i\varphi_\ell] = g\operatorname{Re}\left[\frac{(x + iy)\,{}_1F_1(x + iy + 1, 2x + 1; -iz)}{x\,{}_1F_1(x + iy, 2x; -iz)}\right] = g. \tag{52}$$

Consequently, the energy of the bound states will be determined by $\operatorname{Re}[\varphi_\ell(\varepsilon)] = \operatorname{Re}[\phi_\ell(\varepsilon)]$. This equation does not admit solutions in closed form but they will be analyzed in the next section.

4 General properties of the bound state structure

In the previous section we have established the matching conditions that radial wave functions must fulfill so that the δ and the local δ' interactions are well defined. From that, in this section we consider the complete Hamiltonian (15) and we will draw some relevant conclusions as to the existence and properties of bound states from the secular equation (40). In this secular equation, divergent terms appear for values of the dimensionless energy $\varepsilon \in (0,1)$ when either $W_{\lambda, \frac{1}{2}+\ell}(\eta R) = 0$ or when $_1F_1(a, \ell + \frac{3}{2}; -ig) = 0$. Therefore, it is necessary to analyze the zeros of these functions. Next, we will show that $\phi_\ell(\varepsilon)$, essentially a combination of Whittaker functions, has no singularities for $\varepsilon \in (0,1)$ because the Whittaker function in its denominator has no zeros, and we will also give a good approximation for the zeros of the Kummer function that appears in the denominator of $\varphi_\ell(\varepsilon)$.

4.1 Zeros of the hypergeometric functions

First we want to show that $\phi_\ell(\varepsilon)$ in (44) is a continuous function when $\varepsilon \in (0,1)$, for which we must show that $W_{\lambda, \frac{1}{2}+\ell}(\eta R) = 0$ has no solution in the mentioned interval. Since the Whittaker function can be written in terms of the Tricomi function as

$$W_{\chi, \gamma}(z) = e^{-\frac{1}{2}z} \, z^{\frac{1}{2}+\gamma} \, U\left(\frac{1}{2} + \gamma - \chi, 1 + 2\gamma; z\right), \tag{53}$$

the zeros of $W_{\chi, \gamma}(z)$ are those of $U\left(\frac{1}{2} + \gamma - \chi, 1 + 2\gamma, z\right)$. To prove the absence of positive zeros we use the first theorem of [33], which states that there are no positive zeros z_ν of $U(a_1, a_2; z_\nu) = 0$, if the two real parameters satisfy $2a_1 - a_2 > -1$. In the present case we have $W_{\lambda, \ell+\frac{1}{2}}(\eta r)$, and therefore $2a_1 - a_2 = -2\lambda > -1$ since $\lambda < 0$, so we can conclude that the function $\phi_\ell(\varepsilon)$ is continuous for each value of the angular momentum in the interval $\varepsilon \in (0,1)$.

On the other hand, the function $\varphi_\ell(\varepsilon)$ defined in (43) will not be continuous in the interval $\varepsilon \in (0,1)$ due to the zeros of $_1F_1(a, \ell + \frac{3}{2}; -ig)$, the dependence on ε entering only through a defined in (42). As a good approximation to the a-zeros of this function, $_1F_1(a_n, c; z) = 0$, is given by [29]

$$a_n = -\frac{\pi^2}{4z}\left(n^2 + \left(c - \frac{3}{2}\right)n\right) - \frac{1}{16z}\left(\left(c - \frac{3}{2}\right)^2\pi^2 + \frac{4}{3}z^2 - 8c(z-1) - 4c^2 - 3\right) + \mathcal{O}\left(n^{-1}\right), \quad n \in \mathbb{N}, \tag{54}$$

even for low values of n. In the present case $c = \ell + \frac{3}{2}$, $z = -ig$, and a tedious calculation takes us from (42) and the truncated form of (54) to the following definition

$$\varepsilon_{n\ell} \equiv 1 - \frac{8g^2}{3v_0{}^2} + \frac{\ell}{v_0^2} - \frac{\ell n \pi^2}{v_0^2} - \frac{n^2\pi^2}{v_0^2} - \frac{\ell^2\left(\pi^2 - 4\right)}{4v_0^2} < 1. \tag{55}$$

Therefore, the function $\varphi_\ell(\varepsilon)$ will present a finite number of discontinuities in $\varepsilon \in (0,1)$, which are approximately given by $\varepsilon_{n\ell}$. The typical behavior of the real parts of the $\varphi_\ell(\varepsilon)$ and $\phi_\ell(\varepsilon)$ functions is shown in Figure 1, where the ε values at the intersections of the blue curves with the orange curve correspond to the solutions of the secular equation (40).
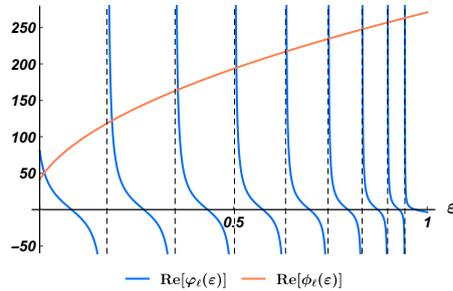
Fig. 1: Bound states from the secular equation (40) for $\ell = 1$, $v_0 = 30$, $w_{\ell j} = -20$, $g = 3.5$, and $\beta = 4$. The dashed vertical lines correspond to the values of $\varepsilon_{n\ell}$ given in (55).

The monotonicity properties of the curves shown in Fig. 1 are due to the fact that

$$\frac{d\varphi_\ell(\varepsilon)}{d\varepsilon} < 0, \qquad \frac{d\phi_\ell(\varepsilon)}{d\varepsilon} > 0. \tag{56}$$

The first inequality holds for all the intervals delimited by the zeros of the function $_1F_1(a_n, \ell + \frac{3}{2}; -ig) = 0$. We have shown the inequalities of (56) for the particular case $g = 0$ in Appendix B.1 of [1], where we have also proved that $\varphi_\ell(\varepsilon)$ is one to one and onto as a function

$$\varphi_\ell(\varepsilon) : I_n \subset (0, 1) \mapsto \mathbb{R}, \ n \in \mathbb{N}, \tag{57}$$

being I_n the interval delimited by two consecutive zeros of $_1F_1(a, \ell + \frac{3}{2}; -ig)$. With the approximation given in (55) we have $I_n \equiv (\varepsilon_{n+1\,\ell}, \varepsilon_{n\ell})$, the interval $(\varepsilon_{1\ell}, 1)$ not being considered, see Fig. 1. In all the examples shown in this work, particularly those necessary for the nuclear model, these properties have been verified (although not rigorously demonstrated). From now on, we will assume that the two inequalities in Eq. (56) are valid.

4.2 Angular momentum dependence

The objective of this section is to study some properties of the number of bound states with angular momentum ℓ, denoted by n_ℓ. Strictly speaking, the total number of bound states is given by $(2\ell + 1)n_\ell$ when we take degeneracy into account. As we can see in Fig. 2, $n_{\ell+1} \leq n_\ell$. In addition, there appears to be a certain $\ell_{\max}$ such that

$$n_{\ell_{\max}} > 0 \quad \text{and} \quad n_{\ell'} = 0 \ \ \forall \ell' \geq \ell_{\max} + 1. \tag{58}$$

This behavior is typical of spherical potentials [34] and was proven for $g = 0$ in [1]. In our case we will use the a-zeros given in (54). Specifically, we analyze the behavior of $\varepsilon_{n\ell}$ with respect to ℓ.
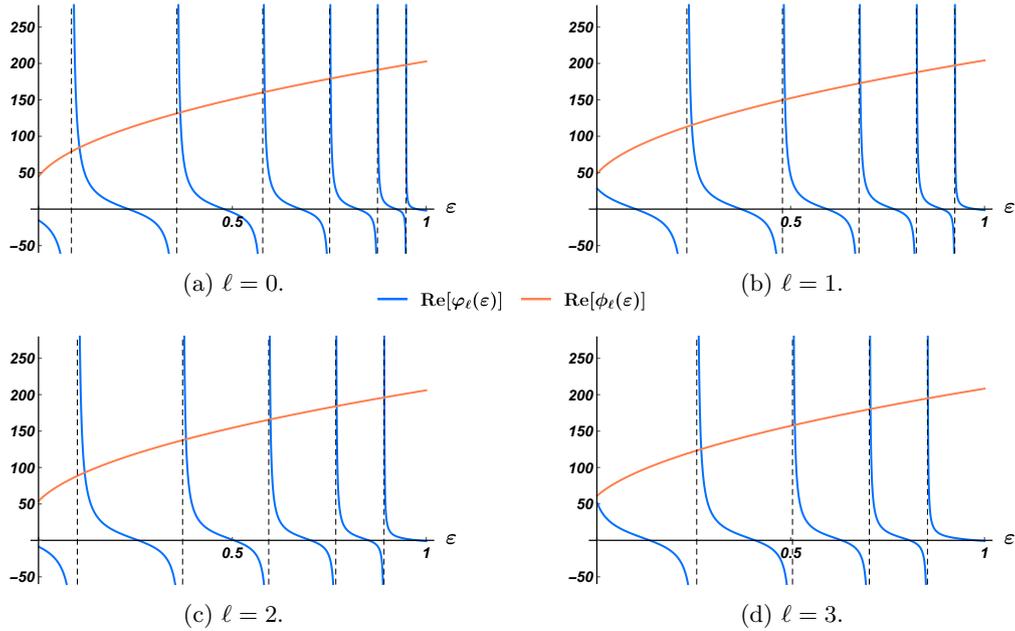
Fig. 2: Bound states from the secular equation (40), $\varphi_\ell(\varepsilon) = \phi_\ell(\varepsilon)$, for $v_0 = 20$, $w_{\ell j} = 20$, $g = 2$ and $\beta = 1$. Note that $w_{\ell j}$ is fixed for all values of ℓ.

We can state that for any $\ell \leq \ell_{\max}$ the number of bound states is given by

$$n_\ell = M + m - m', \tag{59}$$

where M is the number of finite discontinuities of $\varphi_\ell(\varepsilon)$ for $\varepsilon \in (0, 1)$ and

$$m \equiv \begin{cases} 1 & \text{if } \varphi_\ell(0) > \phi(0), \\ 0 & \text{if } \varphi_\ell(0) < \phi(0), \end{cases} \qquad m' \equiv \begin{cases} 1 & \text{if } \phi_\ell(1) < \varphi_\ell(1), \\ 0 & \text{if } \phi_\ell(1) > \varphi_\ell(1). \end{cases} \tag{60}$$

This result, analogous to Theorem 1 in [1], can be proved using the approximation $\varepsilon_{n\ell}$ in (55). First of all, note that the cases $\varphi_\ell(0) = \phi_\ell(0)$ and $\varphi_\ell(1) = \phi_\ell(1)$ are excluded since we are considering energies $\varepsilon \in (0, 1)$. Due to the properties

of $\varphi_\ell(\varepsilon)$ and $\phi_\ell(\varepsilon)$, the number of bound states is primarily determined by the number of discontinuities. For a fixed ℓ these are given by the last value of n such that $\varepsilon_{n\ell} > 0$. Therefore, solving $\varepsilon_{n\ell} = 0$ we obtain

$$M = \max\left\{\left\lfloor \frac{-3\pi\ell + \sqrt{-24g^2 + 9(\ell + \ell^2 + v_0^2)}}{6\pi} \right\rfloor, 0\right\}, \tag{61}$$

where we have assumed $-24g^2 + 9(\ell + \ell^2 + v_0^2) \geq 0$ and $\lfloor \cdot \rfloor$ denotes the floor function so $\varepsilon_{n\ell} \geq 0$. Note that $\varphi_\ell(0) > \phi(0)$ implies the existence of an additional bound state whose energy is the closest to $\varepsilon = 0$. On the other hand, if $\phi_\ell(1) < \varphi_\ell(1)$ there is one less bound state.

The above result is based on approximation (54). In Table 1 we compare approximation (55) with the value obtained by numerically solving $_1F_1(a(\varepsilon), \ell + \frac{3}{2}; -ig) = 0$. In Table 5 of Appendix A we have included similar information for most of the known doubly magic nuclei, verifying that $\varepsilon_{n\ell}$ gives a correct approximation. Furthermore, we have verified for these nuclei that the inequality

$$-24g^2 + 9(\ell + \ell^2 + v_0^2) \geq 0, \tag{62}$$

assumed in the previous proof, is also true.

$\varepsilon_{n\ell}$	$n = 1$		$n = 2$		$n = 3$		$n = 4$		$n = 5$		$n = 6$	
	Num.	App.	Num.	App.	Num.	App.	Num.	App.	Num.	App.	Num.	App.
$\ell = 0$	0.9482	0.9487	0.8745	0.8746	0.7512	0.7513	0.5785	0.5785	0.3565	0.3565	0.0851	0.0851
$\ell = 1$	0.9233	0.9228	0.8243	0.8241	0.6761	0.6761	0.4787	0.4787	0.2320	0.2319	–	–
$\ell = 2$	0.8914	0.8896	0.767	0.7663	0.5939	0.5935	0.3717	0.3715	0.1002	0.1001	–	–
$\ell = 3$	0.8528	0.8491	0.7027	0.7011	0.5046	0.5037	0.2576	0.2569	–	–	–	–
$\ell = 4$	0.8079	0.8013	0.6318	0.6285	0.4084	0.4065	0.1364	0.1351	–	–	–	–
$\ell = 5$	0.7567	0.7461	0.5542	0.5487	0.3054	0.3019	0.0082	0.0059	–	–	–	–

Table 1: Comparison between the approximate values of $\varepsilon_{n\ell}$ that come out of Eq. (55) and the values obtained solving numerically $_1F_1(a(\varepsilon), \ell + \frac{3}{2}; -ig) = 0$, for $v_0 = 20$, $w_{\ell j} = 20$, $g = 2$ and $\beta = 1$.

In Eq. (59), we have assumed the existence of an upper bound for the angular momentum, $\ell_{\max}$. Bargmann inequality [35]

$$n_\ell < \frac{1}{2\ell + 1} \int_0^\infty r|V_-(r)|\, dr, \quad V_-(r) = \min(\{V(r), 0\}), \tag{63}$$

ensures the existence of this upper bound for spherically symmetric potentials satisfying

$$\int_0^\infty |V(r)|\, r^t\, dr < \infty \quad \text{for} \quad t = 1, 2. \tag{64}$$

As explained in [1], due to the δ' interaction, it is not clear how to interpret (63) and Bargmann result can not be used. In any case, using $\varepsilon_{n\ell}$ we can give an approximate value for the maximum value of the angular momentum. Specifically, we investigate the first zero for a given value of the angular momentum, that is, we solve $\varepsilon_{1\ell} = 0$ for ℓ. We got

$$\ell_{\max} = \max\left\{\left\lceil \frac{6 - 6\pi^2 + 2\sqrt{(9\pi^2 - 36)v_0^2 + 9(2\pi^2 + 1) - 24(\pi^2 - 4)g^2}}{3(\pi^2 - 4)} \right\rceil, 0\right\}. \tag{65}$$

This result is analogous to Theorem 2 of [1]. It is worth noting that an increase of v_0, V_0 and R tend to increase $\ell_{\max}$. However, if we boost g, the maximum value of the angular momentum diminish due to the repulsive character of the Coulombic potential. The existence of $\ell_{\max}$ was proved for $g = 0$ in [1]. For the previous example, illustrated in Fig. 2 and Table 1, we have $\ell_{\max} = \lceil 13.34 \rceil = 14$. As it is shown in Fig. 3, in this case the approximation is exact. Note that we have assumed that the inequality

$$(9\pi^2 - 36)v_0^2 + 9(2\pi^2 + 1) - 24(\pi^2 - 4)g^2 \geq 0 \tag{66}$$

holds, which can be verified in Table 6 of Appendix B for all doubly magic nuclei.

(a) $\ell = 14$.   (b) $\ell = 15$.

— $\mathrm{Re}[\varphi_\ell(\varepsilon)]$ — $\mathrm{Re}[\phi_\ell(\varepsilon)]$
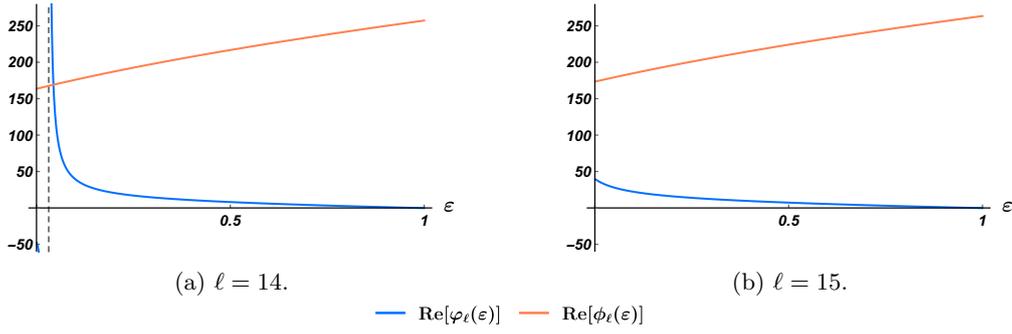
Fig. 3: Plots of $\mathrm{Re}[\varphi_\ell(\varepsilon)]$ (blue) and $\mathrm{Re}[\phi_\ell(\varepsilon)]$ (orange), for $v_0 = 20$, $w_{\ell j} = 20$, $g = 2$ and $\beta = 1$. In (a), for $\ell = 14$, there is an intersection that is a solution of the secular equation, but this does not happen in (b) for $\ell = 15$. Hence, $\ell_{\max} = 14$.

Now, let us focus on the order of the bound states. For spherically symmetric potentials, it can be proved using spectral properties of the Hamiltonian [34] that the energies of bound states characterized by n and ℓ satisfy

$$E_{n\ell} < E_{(n+1)\ell} < E_{(n+1)(\ell+1)}, \quad n, \ell \in \mathbb{N}_0. \tag{67}$$

We extend this result to our case, in which the additional quantum number j is present and, from now on, will be displayed using nuclear spectroscopic notation $n\ell j \equiv n\ell_j$. If there are bound states with relative energies $\varepsilon_{n\ell_j}$, $\varepsilon_{(n+1)\ell_j}$, and $\varepsilon_{n(\ell+1)_j}$ for $n, \ell \in \mathbb{N}_0$, the following inequalities hold:

$$(a) \ -\varepsilon_{n\ell_j} < -\varepsilon_{(n+1)\ell_j}, \qquad (b) \ -\varepsilon_{n\ell_j} < -\varepsilon_{n(\ell+1)_j}, \qquad (c) \ -\varepsilon_{n\ell_{\ell+1/2}} < -\varepsilon_{n\ell_{\ell-1/2}}, \tag{68}$$

a result that was proved for $g = 0$ in [1]. Note that the first inequality is trivial. The second one, which only applies to $j = \ell + 1/2$, follows from the behavior of $\varphi_\ell(\varepsilon)$ and $\phi_\ell(\varepsilon)$ with respect to ℓ. Firstly, if we have $\ell_1 = \ell$ and $\ell_2 = \ell+1$, we need $j_1 = \ell_1 + \frac{1}{2} = \ell + \frac{1}{2}$ and $j_2 = \ell_2 - \frac{1}{2} = \ell + \frac{1}{2}$. Consequently,

$$w_{\ell_1 j_1} = -\frac{2\mu}{\hbar^2}V_{\mathrm{so}}\ell \leq 0, \qquad w_{\ell_2 j_2} = \frac{2\mu}{\hbar^2}V_{\mathrm{so}}(\ell+2) > 0, \tag{69}$$

since $V_{\mathrm{so}} > 0$ [28]. Now, we study how $\varphi_\ell(\varepsilon)$ and $\phi_\ell(\varepsilon)$ vary with respect to ℓ. The generic behavior is illustrated in Fig. 4 for a particular case.
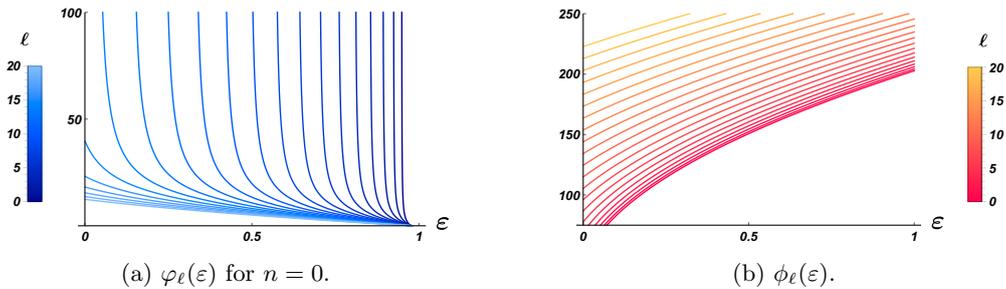
(a) $\varphi_\ell(\varepsilon)$ for $n = 0$.   (b) $\phi_\ell(\varepsilon)$.

Fig. 4: Variation of the two functions defining the secular equation $\mathrm{Re}[\varphi_\ell(\varepsilon)] = \mathrm{Re}[\phi_\ell(\varepsilon)]$ with respect to ℓ for $v_0 = 20$, $w_{\ell j} = 20$, $g = 2$ and $\beta = 1$. In Fig. 4a we have only shown the behavior for $n = 0$, but the same pattern is valid for $n \geq 1$ as can be seen in Figs. 2 and 5.

We analyze the points of intersection between $\varphi_\ell(\varepsilon)$ and $y = y_0 > 0$ for two values of ℓ:

$$\varphi_\ell(\varepsilon) = y_0, \quad \varphi_{\ell'}(\varepsilon') = y_0. \tag{70}$$

Note that for all the proton cases considered in this paper we have $\phi_\ell(\varepsilon) > 0$ in $\varepsilon \in (0, 1)$. This also holds for the nucleus ^{132}Sn used in [1]. Due to the monotonicity and the behavior shown in Fig. 4a, we conclude that $\ell < \ell'$ implies that $\varepsilon > \varepsilon'$. Now, taking into account the Eq. (69) and that $\phi_{\ell+1}(\varepsilon) > \phi_\ell(\varepsilon)$ for any ℓ and $\varepsilon \in (0, 1)$, see Fig. 4b, it follows that the inequality $-\varepsilon_{n\ell_j} < -\varepsilon_{n(\ell+1)_j}$ is necessarily fulfilled. Note that in Fig. 4b we assumed a constant $w_{\ell j}$. For ℓ_2, $w_{\ell_2 j_2} > 0$ and for ℓ_1, $w_{\ell_1 j_1} < 0$, then the quantity $\phi_{\ell+1}(\varepsilon) - \phi_\ell(\varepsilon)$ is even greater than that shown in Fig. 4b.

Finally, the third inequality in (68) is easily proved considering that the dependence on j only enters through $w_{\ell j}/(2-\beta)^2$, being $w_{\ell j_-} > 0$, $w_{\ell j_+} < 0$, where we are considering $\ell > 0$ and $j_\pm \equiv \ell \pm 1/2$.

4.3 Low-lying energy states

As it can be seen from the examples shown in Figs. 1 and 2, $\varepsilon_{n\ell}$ can be reasonably well approximated by the value of the bound state, specially for the first values of n and ℓ:

$$\varepsilon_{n\ell_j} \equiv \varepsilon_{n\ell} = 1 - \frac{8g^2}{3v_0{}^2} + \frac{\ell}{v_0^2} - \frac{\ell\,n\,\pi^2}{v_0^2} - \frac{n^2\pi^2}{v_0^2} - \frac{\ell^2\left(\pi^2-4\right)}{4v_0^2}. \tag{71}$$

We must bear in mind that this approach only considers the a-zeroes of $_1F_1(a_n, \ell + \frac{3}{2}; -ig)$, so it does not depend on $w_{\ell j}$, that is, on j. However, this dependence can be introduced by considering the complete secular equation $\varphi_\ell(\varepsilon) = \phi_\ell(\varepsilon)$ so Eq. (71) can be used to give an easy and analytical proof of the inequalities (68):

○ The inequality $-\varepsilon_{n\ell_j} < -\varepsilon_{(n+1)\ell_j}$ can be shown from (71), as it is clear that $\varepsilon_{n+1\ell} < \varepsilon_{n\ell}$ since the term

$$-\frac{\ell\,n\,\pi^2}{v_0^2} - \frac{n^2\pi^2}{v_0^2} \tag{72}$$

  decreases with n. Consequently, since we are considering $\varepsilon_{n\ell} \simeq \varepsilon_{n\ell_j}$, the inequality is proved.
○ The inequality $-\varepsilon_{n\ell_j} < -\varepsilon_{n(\ell+1)_j}$ is also trivial from Eq. (71) since the terms depending on ℓ are

$$\frac{\ell}{v_0^2} - \frac{\ell\,n\,\pi^2}{v_0^2} - \frac{\ell^2\left(\pi^2-4\right)}{4v_0^2} = -\frac{\ell\left(\pi^2 n - 1\right)}{v_0^2} - \frac{\ell^2\left(\pi^2-4\right)}{4v_0^2}, \tag{73}$$

  and this quantity decreases with ℓ.
○ Let us consider finally the inequality $-\varepsilon_{n\ell_{\ell+1/2}} < -\varepsilon_{n\ell_{\ell-1/2}}$. As mentioned before, the dependence on j only enters through $w_{\ell j}/(2-\beta)^2$, being $w_{\ell j} > 0$ for $j = \ell - \frac{1}{2}$ and $w_{\ell j} < 0$ for $j = \ell + \frac{1}{2}$. Since we are considering $\ell > 0$, it is clear that we can write

$$-\varepsilon_{n\ell_{\ell+1/2}} \lesssim -\varepsilon_{n\ell_{\ell-1/2}}. \tag{74}$$

Note that the approximation of Eq. (71) could be no longer valid if $w_{\ell j} \ll 0$ such that $\phi_\ell(1) \approx 0$.

5 Proton and neutron energy levels of ^{208}Pb

This section is dedicated to applying the above framework to a realistic physical situation. To do this, we choose the free parameters values of our potential that have been shown in order to mimic certain nuclei. In particular, for this phenomenological potential the usual parametrization is [28]

$$R = r_0 A^{1/3} = 1.27 A^{1/3} \text{ fm}, \qquad V_0 = \left(51 \pm 33\frac{N-Z}{A}\right) \text{ MeV}, \qquad V_{\text{so}} = 0.44V_0 \text{ fm}, \tag{75}$$

where the $+$ sign is for a proton and the $-$ sign for a neutron. This model is particularly useful for doubly magic nuclei. Consequently, we will exemplify the procedure with the nucleus ^{208}Pb. In Appendix B the same procedure is applied to ^{40}Ca and ^{16}O. We have illustrated with Pb since it has the largest number of bound states. Our objective is to show that the low-lying bound states level scheme obtained from our model is quite reasonable for the isotopes considered. A high-precision numerical fit is beyond the purpose of the model.

To begin with, in Table 2 we show the physical constants and dimensionless quantities needed for these three nuclei. The parameter β, the intensity of the δ' term, is not fixed and in fact we will use it to adjust the results to fit the data available for the above isotopes.

Next, for ^{208}Pb we determine the neutron and proton energy levels for $\ell = 0, 1$ setting $\beta = 0$. In Fig. 5 we show the points of intersection in this case. Using nuclear spectroscopic notation we compare the data obtained here with the neutron and proton energy levels found in [36], where the usual parameters of the Woods-Saxon (WS) model are optimized to obtain the best fit with the available experimental data. The results are shown in Table 3. From the results on this table, we see the inequalities demonstrated in Sec. 4 are valid for both cases:

$$|E(ns_{1/2})| > |E(np_{1/2})|, \qquad |E(np_{3/2})| > |E(np_{1/2})|. \tag{76}$$

We also observe that the energy values decrease with n. In general, for all the isotopes considered in this work we have $|E(n\ell_{\ell-1/2})| < |E(n\ell_{\ell+1/2})|$, as expected from Eq. (68). It should be mentioned that this is the opposite behavior to that found for electrons. In fact, the nucleon that is aligned with the orbital angular momentum is attracted more strongly. The explanation of all the experimental magic number was finally possible when the spin-orbit interaction

	^{208}Pb		^{40}Ca		^{16}O	
	Proton	Neutron	Proton	Neutron	Proton	Neutron
R/fm	7.542		4.343		3.200	
V_0/MeV	57.98	44.02	51.00		51.00	
V_{so}/MeV fm	25.51	19.36	22.44		22.44	
$w_{\ell j}$ $w_{\ell j_+}$	$-18.43\,\ell$	$-13.99\,\ell$	$-9.361\,\ell$		$-6.897\,\ell$	
$w_{\ell j_-}$	$18.43(\ell+1)$	$13.99(\ell+1)$	$9.361(\ell+1)$		$6.897(\ell+1)$	
g	4.621	0	1.730	0	0.939	0
v_0	12.56	10.94	6.797		5.008	

Table 2: Physical constants and dimensionless quantities needed to calculate the proton and neutron level scheme of the three isotopes ^{208}Pb, ^{40}Ca and ^{16}O.
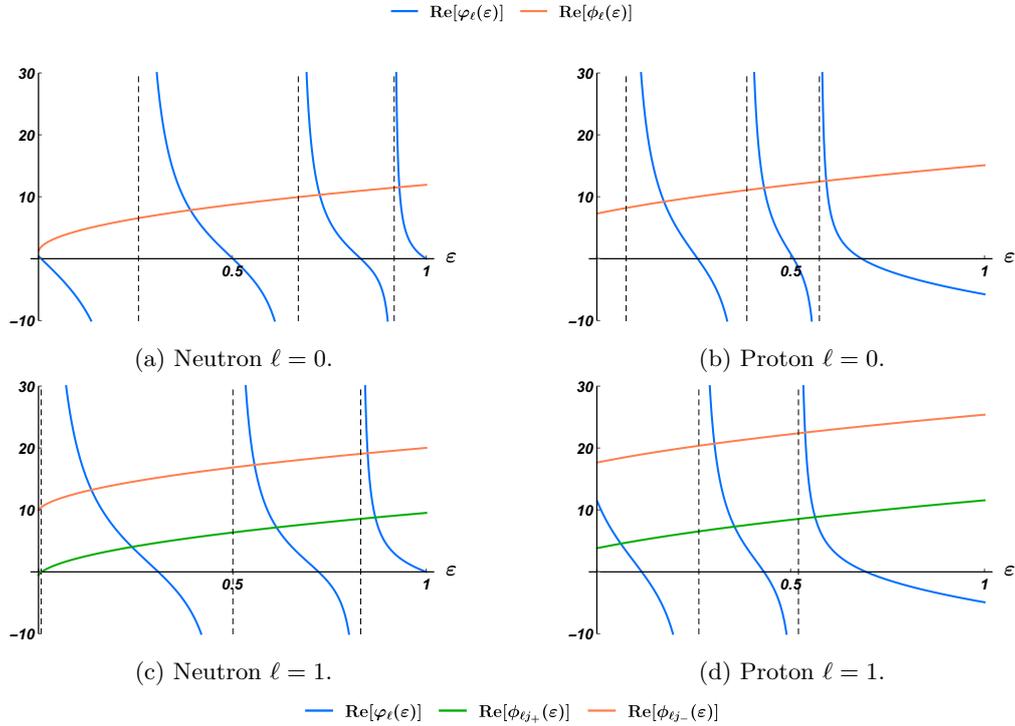
Fig. 5: Bound states for ^{208}Pb from the secular equation (40), $\text{Re}[\varphi_\ell(\varepsilon)] = \text{Re}[\phi_\ell(\varepsilon)]$, with $\beta = 0$. As can be seen, the bound states of a neutron are more deeply bound than those of a proton. Precise values are shown in Table 3.

was included in the mean-field shell model. It is also worth noting that the energy values of neutron are deeper than those of protons as we can see in Fig. 5. This can be partly explained by Coulomb's repulsive term in the potential. However, since $N > Z$ for this nucleus, note that V_0 is larger for protons, as can be see in (75). The latter is the result of the average nucleon-nucleon potential, which is stronger for the proton-neutron interaction than the neutron-neutron or proton-proton case. Consequently, V_{so} is also different for protons and neutrons. For other nuclei without a neutron excess, ^{40}Ca or ^{16}O, protons will not feel a stronger potential well than neutrons.

Now we are going study the effect of the δ' term for ^{208}Pb. From a phenomenological point of view, it can be used to improve the level scheme given by our model with just the Dirac δ. We denote by $E_\beta(n\ell_j)$ the energy of the state characterized by $\{n, \ell, j, \beta\}$, being $E_{\text{WS}}(n\ell_j)$ the corresponding energy arising from the optimized Woods-Saxon model in [36]. To measure the amount of dispersion for this set of values we define

$$\sigma_\beta \equiv \sqrt{\frac{1}{N} \sum_{n\ell_j} [E_\beta(n\ell_j) - E_{\text{WS}}(n\ell_j)]^2}, \tag{77}$$

State	$E_{\text{neutr.}}$/MeV.		$E_{\text{prot.}}$/MeV.	
	$\beta = 0$	WS	$\beta = 0$	WS
$0s_{1/2}$	−40.98	−39.62	−34.30	−31.73
$1s_{1/2}$	−31.94	−29.19	−25.02	−21.26
$2s_{1/2}$	−17.25	−14.81	−10.04	−6.58
$0p_{3/2}$	−38.25	−36.01	−32.63	−28.71
$1p_{3/2}$	−27.03	−23.22	−20.58	−15.19
$2p_{3/2}$	−10.61	−7.97	−3.57	−
$0p_{1/2}$	−37.37	−35.05	−31.14	−27.82
$1p_{1/2}$	−24.53	−22.22	−17.57	−14.42
$2p_{1/2}$	−6.01	−6.93	−	−

Table 3: Proton and neutron level scheme of ^{208}Pb arising from our model with $\beta = 0$ compared to that of the optimized Woods-Saxon model developed in [36].

where N is the number of states. In Fig. 6 we have represented this quantity as a function of β and it is obvious that there are values of β that minimize this variation. We have focused on the values that minimize σ_β and the results

(a) Neutron.

(b) Proton.

(c) Neighborhood of the value minimizing σ_β for neutrons.

(d) Neighborhood of the value minimizing σ_β for protons.
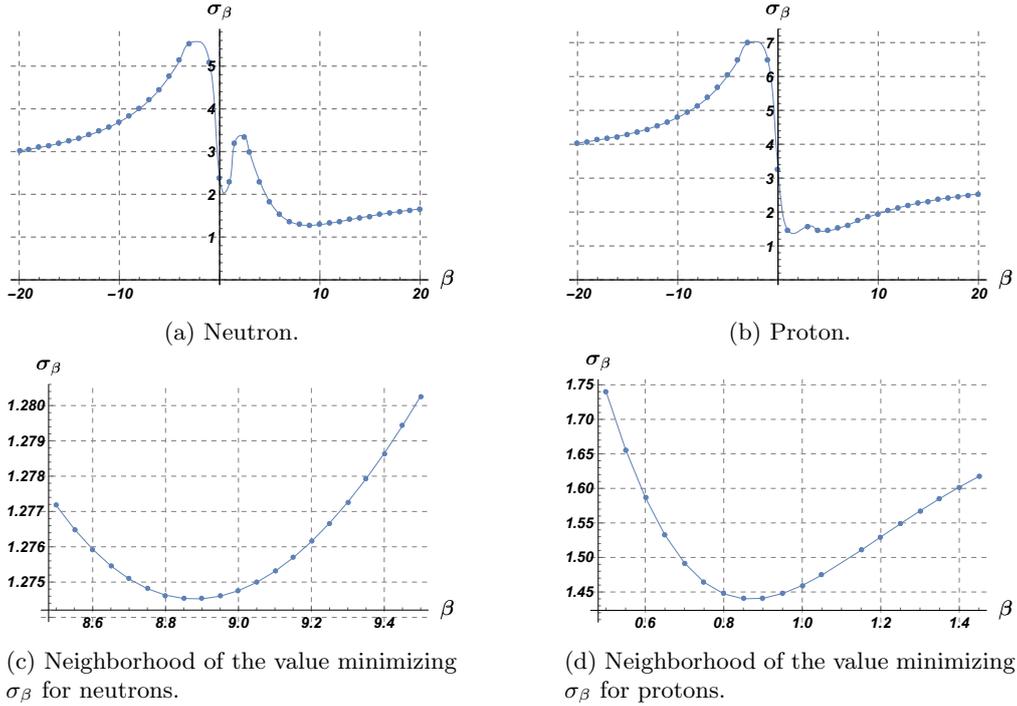
Fig. 6: Values of the dispersion σ_β (77) for the nucleus ^{208}Pb.

are shown in Table 4. Note that the values $\beta = 0$ and $\beta = 1$ correspond to $V_q = 0$ and $V_q = -20.83$ MeV fm^2, respectively. It is clear that the introduction of a non-trivial β allows us to better reproduce the level scheme found with the Woods-Saxon model.

6 Concluding remarks

In this work, we have extended a previous study on a nuclear model based on an interaction due to a three-dimensional Dirac δ and local δ', allowing the presence of the Coulombic term due to the electromagnetic interaction between

State	$E_{\text{neutr.}}$/MeV.			$E_{\text{prot.}}$/MeV.		
	$\beta = 0$	$\beta = 8.9$	WS	$\beta = 0$	$\beta = 0.85$	WS
$0s_{1/2}$	-40.97	-40.65	-39.62	-34.30	-33.46	-31.73
$1s_{1/2}$	-31.93	-30.67	-29.19	-25.02	-22.95	-21.26
$3s_{1/2}$	-17.25	-14.81	-14.81	-10.03	-5.84	-6.58
$0p_{3/2}$	-38.25	-37.14	-36.01	-32.63	-30.53	-28.71
$1p_{3/2}$	-27.03	-24.02	-23.22	-20.58	-16.34	-15.19
$2p_{3/2}$	-10.61	-6.25	-7.97	$-$	$-$	$-$
$0p_{1/2}$	-37.37	-37.13	-35.05	-31.14	-30.37	-27.82
$1p_{1/2}$	-24.53	-23.95	-22.22	-17.57	-15.82	-14.42
$2p_{1/2}$	-6.09	-6.02	-6.93	$-$	$-$	$-$

Table 4: Proton and neutron level scheme of ^{208}Pb arising from our model with $\beta = 0$ and the optimal β compared to that of the optimized Woods-Saxon model developed in [36].

protons. From a mathematical point of view, this contact potential has been precisely defined using suitable matching conditions satisfied by the radial wave functions. We have obtained general properties relative to the number and behavior of bound states of the aforementioned nuclear potential. As expected from what we know about spherically symmetric potentials, the eigenstates are less bound if we increase n or the angular momentum, the other quantum numbers being fixed. We have also shown that there is a maximum value of ℓ, so that consequently there is a finite number of bound states, since the number of them, for a given value of ℓ, is finite. We have given an estimate of these two quantities, $\ell_{\max}$ and n_ℓ. We have analyzed the effect of the spin-orbit interaction, obtaining that the state with $j = \ell + 1/2$ is more bounded than the one with $j = \ell - 1/2$, as expected from considerations on the shell model. For the lowest energy states, those near the bottom of the well, all these properties have been analytically tested.

In the last section we used this model to approximately describe the single-particle neutron and proton energy levels of the doubly magic nucleus ^{208}Pb. We have shown that the Hamiltonian (14), based on the Woods-Saxon potential with the surface diffuseness going to zero, provides a fair approximation for the low-lying bound states. The δ term gives the nuclear spin-orbit contribution. The aim of the additional interaction, given by the local δ', is providing a correction such that the results of the proposed model better fit to the available data. In these sense, we have determined which is the best value of the δ' coupling, β, for the nucleon and proton energy levels in the three nuclei ^{208}Pb, ^{40}Ca and ^{16}O. In particular, we have focused on ^{208}Pb, comparing our level scheme for nucleons with a Woods-Saxon model in which the free parameters as a and r_0 are not the usual, but those optimized in order to fit with the available experimental data. As we have seen, the introduction of the δ' interaction does not change the fundamental properties of the level scheme. This interaction is initially justified for the construction of a self-adjoint extension of the Hamiltonian but, as we have seen, it can be used to improve numerical precision. This justifies the choice of the so called local δ' interaction. Note that the other possible choice for the δ' interaction is not compatible with the Dirac δ if both are supported at $r = R$. We have proved that the latter is a requirement when the starting point is Woods-Saxon potential.

This simplified model could be used to gain insight into the proton and neutron energy levels for doubly magic nuclei. In this sense, the case studied in [1] could be seen as a particular case, $Z = 0$, of the present model. In both cases, the main advantage over the Woods-Saxon potential is that the eigenfunction equation can be solved exactly, obtaining analytic properties of the spectrum using well-known features of special functions: for $Z \neq 0$ the solution is given in terms of hypergeometric functions with complex arguments, while for $Z = 0$ the solution reduces to the usual Bessel functions. In the latter, it is easier to take advantage of known results in order to prove the desired properties of the bound state structure, as was done in [1]. However, hypergeometric functions with complex arguments are not as well studied in the scientific literature, so a rigorous analysis of the $Z \neq 0$ case has not been possible and a more qualitative study has been carried out instead.

Acknowledgments

Appendix A

In this appendix we compute several quantities appearing in the text for all the known doubly magic nuclei. We begin with the approximation made for the a-zeros of $_1F_1(a_n, \ell + \frac{3}{2}; -ig)$ in (55), the points where the function $\phi_\ell(\varepsilon)$ presents a finite number of discontinuities in $\varepsilon \in (0, 1)$. As we see in Table 5, this is a fair approximation for the isotopes we are interested in. The isotope ^{4}O is not included since $\varepsilon_{n\ell} < 0$ for all cases. From the approximation given in Table 5

$\varepsilon_{n\ell}$		$n = 1$		$n = 2$	
		Num.	App.	Num.	App.
^{10}O	$\ell = 0$	0.07440	0.07524	–	–
^{16}O	$\ell = 0$	0.5110	0.5127	–	–
	$\ell = 1$	0.1027	0.1006	–	–
^{40}Ca	$\ell = 0$	0.6106	0.6136	–	–
	$\ell = 1$	0.3930	0.3899	–	–
	$\ell = 2$	0.1152	0.1026	–	–
^{48}Ca	$\ell = 0$	0.6023	0.6056	–	–
	$\ell = 1$	0.3868	0.3835	–	–
	$\ell = 2$	0.1112	0.09829	–	–
^{48}Ni	$\ell = 0$	0.6203	0.6238	0.1103	0.1114
	$\ell = 1$	0.4486	0.4449	–	–
	$\ell = 2$	0.2281	0.2153	–	–
^{56}Ni	$\ell = 0$	0.6095	0.6131	0.0999	0.1011
	$\ell = 1$	0.4383	0.4344	–	–
	$\ell = 2$	0.2181	0.2048	–	–
^{78}Ni	$\ell = 0$	0.5918	0.5958	0.0922	0.09352
	$\ell = 1$	0.4247	0.4204	–	–
	$\ell = 2$	0.2094	0.1953	–	–
^{100}Sn	$\ell = 0$	0.5611	0.5658	0.2159	0.2178
	$\ell = 1$	0.4504	0.4443	–	–
	$\ell = 2$	0.3047	0.2883	–	–
	$\ell = 3$	0.1268	0.09789	–	–
^{132}Sn	$\ell = 0$	0.5367	0.5416	0.1965	0.1986
	$\ell = 1$	0.4285	0.4218	–	–
	$\ell = 2$	0.2856	0.2681	–	–
	$\ell = 3$	0.1108	0.08042	–	–
^{208}Pb	$\ell = 0$	0.439	0.4436	0.1926	0.1962
	$\ell = 1$	0.3678	0.3572	0.02930	0.02738
	$\ell = 2$	0.2695	0.2463	–	–
	$\ell = 3$	0.1471	0.1109	–	–
	$\ell = 4$	0.0020	0.0490	–	–

Table 5: Values of $\varepsilon_{n\ell}$ for all the double-magic nuclei.

we have derived that the maximun number of bound states for a given value of the angular momentum is mainly given by M in (61). We have found that the maximum value of the angular momentum allowed in the system can be approximated by

$$\ell_{\max} = \max \left\{ \left\lceil \frac{6 - 6\pi^2 + 2\sqrt{(9\pi^2 - 36)\, v_0^2 + 9\,(2\pi^2 + 1) - 24\,(\pi^2 - 4)\, g^2}}{3\,(\pi^2 - 4)} \right\rceil, 0 \right\}.$$

Both depend on the dimensionless quantities v_0 and g, which are also calculated for these nuclei. Note that both radicands

$$r_1 \equiv -24g^2 + 9(\ell + \ell^2 + v_0^2), \qquad r_2 \equiv (9\pi^2 - 36)\, v_0^2 + 9\,(2\pi^2 + 1) - 24\,(\pi^2 - 4)\, g^2, \qquad \text{(A.1)}$$

must be positive, which is in effect shown in Table 6 for all isotopes considered here.

Nucleus	Z	N	v_0 (proton)	v_0 (neutron)	g	$R/$ fm	r_1	r_2
$^{4}_{2}\text{He}$	2	2	3.155	3.155	0.372	2.016	86.254	692.930
$^{10}_{2}\text{He}$	2	8	5.045	3.349	0.434	2.736	96.429	752.656
$^{16}_{8}\text{O}$	8	8	5.008	5.008	0.939	3.200	204.568	1387.390
$^{40}_{20}\text{C}$	20	20	6.797	6.797	1.730	4.343	343.957	2205.540
$^{48}_{20}\text{Ca}$	20	28	7.603	6.823	1.784	4.615	342.555	2197.320
$^{48}_{28}\text{Ni}$	28	20	6.823	7.602	2.110	4.615	413.283	2612.460
$^{56}_{28}\text{Ni}$	28	28	7.604	7.604	2.165	4.858	407.827	2580.430
$^{78}_{28}\text{Ni}$	28	50	9.235	7.678	2.288	5.426	404.871	2563.080
$^{100}_{50}\text{Sn}$	50	50	9.225	9.225	3.187	5.894	522.076	3251.030
$^{132}_{50}\text{Sn}$	50	82	10.885	9.292	3.338	6.466	509.584	3177.710
$^{208}_{82}\text{Pb}$	82	126	12.557	10.940	4.612	7.524	566.677	3512.820

Table 6: Dimensionless quantities and radius for all the doubly magic nuclei. As we can see, $r_1, r_2 > 0$.

Appendix B   Proton and neutron energy levels of ^{40}Ca and ^{16}O

The same procedure as in Sec. 5 can be applied to the doubly magic nuclei ^{40}Ca and ^{16}O. We will use the usual parametrization [28]: $R = r_0 A^{1/3} = 1.27 A^{1/3}$ fm, $V_0 = 51$ MeV, and $V_{\text{so}} = 0.44 V_0$ fm. From Table 6 we see that, contrary to ^{208}Pb, the number of protons and neutrons is the same for these two isotopes, so we use the same potential depth, $V_0 = 51$ MeV, for both level schemes. From this table we can also obtain the dimensionless quantities necessary for the calculation of the bound states:

$$^{40}\text{Ca}: \quad v_0 \approx 6.797, \ g \approx 1.730 \quad \text{and} \quad w_{\ell j} = -\frac{8\mu R}{\hbar^2} V_{\text{so}}\, \xi_{\ell j} \approx -18.723\, \xi_{\ell j},$$

$$^{16}\text{O}: \quad v_0 \approx 5.008, \ g \approx 0.939 \quad \text{and} \quad w_{\ell j} = -\frac{8\mu R}{\hbar^2} V_{\text{so}}\, \xi_{\ell j} \approx -13.795\, \xi_{\ell j}.$$

In this case we will compare with the data obtained from the usual Woods-Saxon model [28], and not with an optimized one as in Sec. 5. We can evaluate σ_β, which was defined in Eq. (77) and is represented in Figs. 7 and 8. In both cases, σ_β is similar for protons and neutrons. Unlike ^{208}Pb, the best value of β for neutrons is obtained before the peak at $\beta = 2$ and after this peak for protons. Remember that for the values $\beta = \pm 2$ the matching conditions (38) are ill-defined and we have to use the conditions (39). It is observed that, as happened in Section 5, negative values of β give rise to greater dispersion. Once we have obtained the best values of β we can compare the resulting level scheme with the one in the absence of the δ' term ($\beta = 0$), and with the one that arises from the regular Woods-Saxon model, which is done in Tables 7 (^{40}Ca) and 8 (^{16}O). For these nuclei, the inequalities with respect to the three quantum numbers derived in Sec. 4, Eq. (68), hold. Specifically, with respect to n we get:

$$|E(0s_{1/2})| > |E(1s_{1/2})|, \qquad |E(0p_{3/2})| > |E(1p_{3/2})|.$$

For ^{16}O there are no bound states to prove the second inequality. Regarding ℓ, in both cases we obtain $|E(0s_{1/2})| > |E(0p_{1/2})|$. Note that the inequality $|E(1s_{1/2})| > |E(1p_{1/2})|$ can not be tested since there are no bound states with $n = 1$, $\ell = 1$ and $j = 1/2$. For ^{208}Pb this states are present, as can be seen in Table 3. With respect to j, we obtain the expected result for the nucleon that is aligned with the orbital angular momentum $\ell = 1$: $|E(0p_{3/2})| > |E(0p_{1/2})|$. As with the previous results, note that for ^{208}Pb it is also possible to test the above inequality for $n = 1$, see Table 3. This is why we have used this nucleus to test our model based on the δ-δ' contact interaction in Sec. 5.

References

1. C. Romaniega, M. Gadella, R. M. Id Betan, L. M. Nieto, Eur. Phys. J. Plus **135**, 372 (2020)

(a) Neutrons.

(b) Protons.

(c) Neighborhood of the value minimizing σ_β for neutrons.

(d) Neighborhood of the value minimizing σ_β for protons.
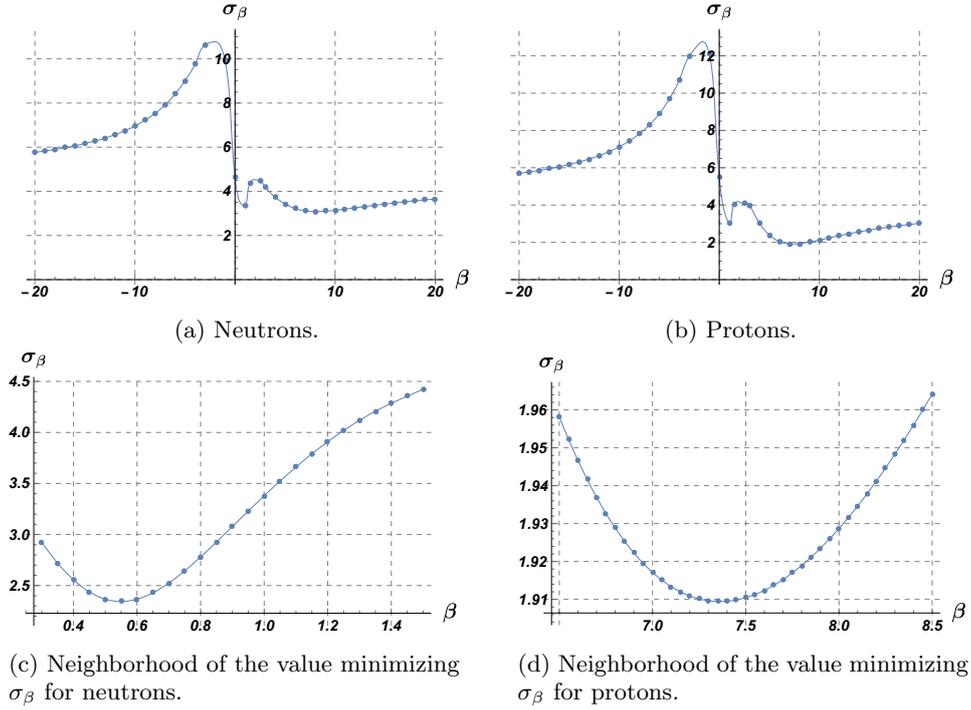
Fig. 7: Values of the dispersion σ_β in Eq. (77) for the nucleus ^{40}Ca.

State	$E_{\text{neutr.}}$/MeV.			$E_{\text{prot.}}$/MeV.		
	$\beta = 0$	$\beta = 0.5$	WS	$\beta = 0$	$\beta = 7.45$	WS
$0s_{1/2}$	-42.782	-41.166	-38.842	-34.156	-32.363	-29.982
$1s_{1/2}$	-19.147	-14.362	-15.684	-10.856	-5.809	-7.990
$0p_{3/2}$	-36.151	-31.778	-29.541	-28.135	-22.763	-21.255
$1p_{3/2}$	-8.199	-4.149	-5.673	$-$	$-$	1.092
$0p_{1/2}$	-31.354	-30.488	-26.942	-23.972	-22.133	-18.573
$1p_{1/2}$	$-$	$-$	-3.320	$-$	$-$	$-$

Table 7: Proton and neutron level scheme of ^{40}Ca arising from our model with $\beta = 0$ and the optimal β, compared with the one from the regular Woods-Saxon model [28].

2. E. Yazdankish, Int. J. Mod. Phys. E **29**, 2050032 (2020)
3. M. Belloni and R.W. Robinett, Phys. Rep. **50**, 25122 (2014)
4. Yu N. Demkov and V.N. Ostrovskii, *Zero-range Potentials and Their Applications in Atomic Physics* (Plenum Press, New York, 1988)
5. S. Albeverio, F. Gesztesy, R. Hoegh-Krohn and H. Holden, *Solvable Models in Quantum Mechanics, 2nd ed.* (AMS Chelsea Publishing, Providence RI, 2004)
6. R. de L. Kronig and W.G. Penney, Proc. R. Soc. Lond. Ser. A **130**, 499 (1931)
7. C. Kittel, *Introduction to Solid State Physics, 8th ed.* (John Wiley & Sons, Inc., 2005)
8. F. Erman, M. Gadella, S. Tunalı, and H. Uncu, Eur. Phys. J. Plus **132**, 352 (2017)
9. H. Uncu, D. Tarhan, E. Demiralp and Ö.E. Müstecaplıoğlu, Phys. Rev. A **76**, 013618 (2007)
10. F. Ferrari, V.G. Rostiashvili and T.A. Vilgis, Phys. Rev. E **71**, 061802 (2005)
11. I. Alvarado-Rodríguez, P. Halevi and J.J. Sánchez-Mondragón, Phys. Rev. E **59**, 3624 (1999)
12. J.R. Zurita-Sánchez and P. Halevi, Phys. Rev. E **61**, 5802 (2000)
13. Lin Ming-Chieh and Jao Ruei-Fu, Phys. Rev. E **74**, 046613 (2006)
14. I. Cavero-Peláez, J. M. Munoz-Castaneda, C. Romaniega, Phys. Rev. D **103**, 045005 (2021)
15. M. Gadella M, J. Negro J and L.M. Nieto, Phys. Lett. A **373**, 1310 (2009)
16. S. Albeverio, S. Fassari and F. Rinaldi, J. Phys. A: Math. Theor. **49**, 025302 (2016)
17. S. Fassari, M. Gadella, M.L. Glasser and L.M. Nieto, Ann. Phys. **389**, 48 (2018)

(a) Neutrons.

(b) Protons.

(c) Neighborhood of the value minimizing σ_β for neutrons.

(d) Neighborhood of the value minimizing σ_β for protons.
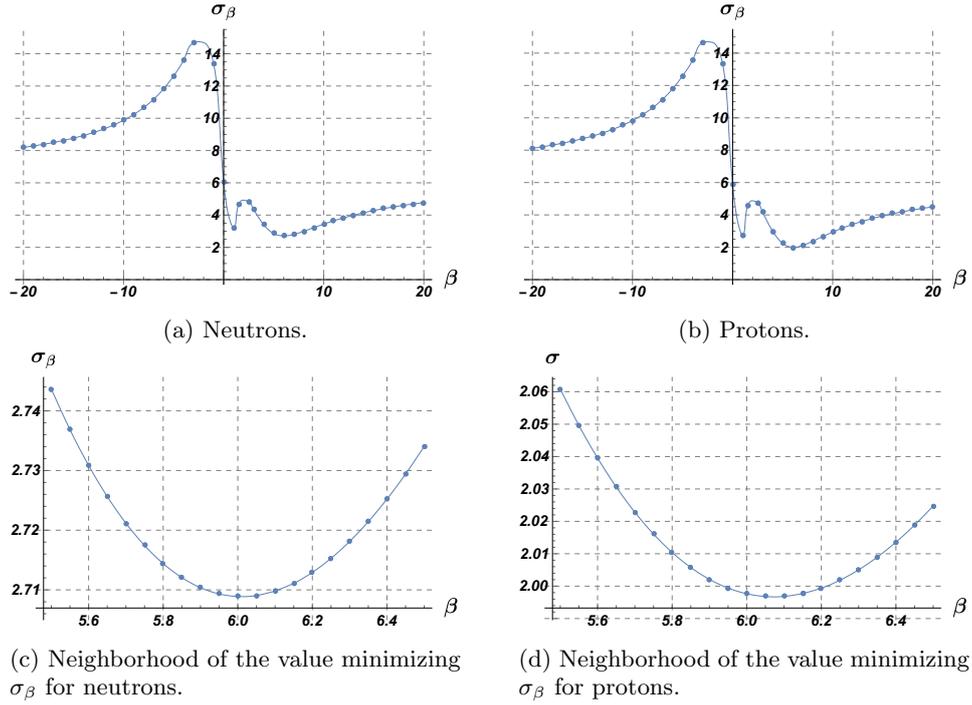
Fig. 8: Values of the dispersion σ_β (77) for the nucleus ^{16}O.

State	$E_{neutr.}$/MeV.			$E_{prot.}$/MeV.		
	$\beta = 0$	$\beta = 3.05$	WS	$\beta = 0$	$\beta = 6.05$	WS
$0s_{1/2}$	-37.292	-33.181	-31.091	-30.462	-28.337	-26.445
$1s_{1/2}$	-1.974	-0.267	-3.970	$-$	$-$	-0.709
$0p_{3/2}$	-27.015	-15.917	-18.612	-22.815	-11.561	-14.451
$0p_{1/2}$	-19.145	-15.470	-14.466	-14.708	-11.088	-9.328

Table 8: Proton and neutron level scheme of ^{16}O arising from our model with $\beta = 0$ and the optimal β, compared with the one from the regular Woods-Saxon model [28].

18. P. Kurasov, J. Math. Anal. Appl. **201**, 297 (1996);
19. M. Gadella, M.L. Glasser and L.M. Nieto, Int. J. Theor. Phys. **50**, 2144 (2011); Int. J. Theor. Phys. **50**, 2191 (2011)
20. J.M. Muñoz-Castañeda, L.M. Nieto and C. Romaniega, Ann. Phys. **400**, 246 (2019)
21. R. de la Madrid, Nucl. Phys. A **962**, 24 (2017)
22. R.M. Id Betan and R. de la Madrid, Nucl. Phys. A **970**, 398 (2018)
23. R.D. Woods and D.S. Saxon, Phys. Rev. **95**, 577 (1954)
24. T. Vertse, K.F. Pal and Z. Balogh, Comp. Phys. Comm. **27**, 309 (1982)
25. B. Gyarmati, K.F. Pal and T. Vertse, Phys. Lett. **104**, 177 (1981)
26. R. Machleidt, *Computational Nuclear Physics Nuclear Reactions*, K. Langanke, J.A. Maruhn and S.E. Koonin eds.(Springer, New York, 1993) p. 1.
27. A. Bohr and B.R. Mottelson, *Nuclear Structure, vol 1* (Benjamin, New York, 1969)
28. J. Suhonen, *From Nucleons to Nucleus* (Springer, New York, 2007)
29. F.W.J. Olver, *NIST Handbook of Mathematical Functions* (Cambridge Univ. Press, New York, 2010)
30. M. Gadella, J.M. Mateos-Guilarte, J.M. Muñoz-Castañeda and L.M. Nieto, J. Phys. A: Math. Theor. **49**, 015204 (2016)
31. J.J. Alvarez, M. Gadella and L.M. Nieto, Int. J. Theor. Phys. **50**, 2161 (2011); J.J. Alvarez, M. Gadella, L.P. Lara and F.H. Maldonado-Villamizar, Phys. Lett. A **377**, 2510 (2013)
32. M. Reed and B. Simon, *Fourier Analysis. Self Adjointness* (Academic Press, New York, 1975)
33. J. Wimp, Proc. Am. Math. Soc. **16**, 281–283, (1965).
34. A. Galindo and P. Pascual, *Quantum Mechanics I (Texts and Monographs in Physics)* (Springer-Verlag, Berlin, 1990)
35. V. Bargmann, Proc. Nat. Acad. Sci. **38**, 961 (1952)
36. A. Sharma, S. Gora, J. Bhagavathi, and O. S. K .S. Sastri, *Am. J. Phys.* **88**, 576 (2020)